Magnetic Resonance in Medicine 63:858–864 (2010)

Systolic 3D First-Pass Myocardial Perfusion MRI: Comparison With Diastolic Imaging in Healthy Subjects

Taehoon Shin,[1]* Gerald M. Pohost,[1,2] and Krishna S. Nayak[1,2]

Three-dimensional (3D) first-pass myocardial perfusion imaging (MPI) is a promising alternative to conventional two-dimensional multislice MPI due to its contiguous spatial coverage that is beneficial for estimating the size of perfusion defects. Data acquisition at mid-diastole is a typical choice for 3D MPI yet is sensitive to arrhythmia and variations in R-R interval that are common in cardiac patients. End systole is the second longest quiescent cardiac phase and is known to be less sensitive to the R-R variability. Therefore, 3D MPI with systolic acquisition may be advantageous in patients with severe arrhythmia once it is proven to be comparable to diastolic MPI in subjects with negligible R-R variation. In this work, we demonstrate the feasibility of 3D MPI with systolic data acquisition in five healthy subjects. We performed 3D MPI experiments in which 3D perfusion data were acquired at both end-systole and mid-diastole of every R-R interval and analyzed the similarity between resulting time intensity curves (TIC) from the two data sets. The correlation between systolic and diastolic TICs was extremely high (mean = 0.9841; standard deviation = 0.0166), and there was a significant linear correlation between the two time intensity curve upslopes and peak enhancements ($P < 0.001$). Magn Reson Med 63:858–864, 2010. © 2010 Wiley-Liss, Inc.

Key words: myocardial perfusion; systolic acquisition; 3D imaging; cardiac MRI; sensitivity encoding

MR first-pass myocardial perfusion imaging (MPI) is an established tool for the clinical assessment of myocardial perfusion because of its high spatial resolution and the lack of exposure to ionizing radiation. The most widely used protocols involve two-dimensional (2D) multislice acquisitions and have been shown to identify the presence of angiographically significant coronary artery disease with high sensitivity (>85%) and specificity (>75%) (1,2). One limitation of two-dimensional multislice protocols is that they provide only partial coverage of the left ventricle (LV), leaving room for potential improvements in diagnosis and prediction of outcomes via increased coverage.

Three-dimensional (3D) MR MPI is a promising alternative to 2D multislice approach due to its contiguous spatial coverage. 3D MPI has been recently shown to be more accurate than 2D multislice technique in estimating the size of defects (3), which is crucial for prognosis in symptomatic patients, as validated by patient follow-up studies (4–7). Additional advantages of 3D MPI include high signal-to-noise ratio (SNR), imaging of all myocardium at a single cardiac phase, a potentially long saturation recovery time, and the capacity for high-rate parallel imaging (3,8). Typically, the acquisition window is positioned at mid-diastole where the heart is the most stationary within an R-R interval. In healthy subjects, previous 3D MPI studies have used ~300-ms acquisition (3,8), although the optimal duration and timing of the acquisition tends to vary over subjects (9).

End-systole is another cardiac phase well suited for data acquisition in MR MPI. It is a shorter quiescent period compared to mid-diastole but is less sensitive to R-R variability and arrhythmia (10). In normal subjects, the duration and timing of diastasis is known to vary more significantly than the duration and timing of end-systole, as a function of heart rate (11). For example, an increase in heart rate from 80 to 90 beats/min results in 5.6% and 16.4% decreases in the duration of systole and diastole, respectively. Systolic data acquisition is likely to be more robust in patients with atrial fibrillation, the most common cardiac arrhythmia, with a prevalence of 9% in elderly people (>65 years) with cardiovascular disease (12). In patients with chronic atrial fibrillation, mean variations in systolic and diastolic time intervals were reported to be 10.6% and 37.9%, respectively (13). A change in the duration and timing of a stable period induces either motion artifacts when data are acquired as scheduled or loss of temporal resolution when data are rejected. Note that the myocardium is thicker at the systole. Thus, lower in-plane spatial resolution may be tolerated, which, to some extent, compensates for the reduction in available acquisition time compared to diastole.

In this paper, we investigate the feasibility of 3D MPI with data acquisition at end-systole and compare it to 3D MPI with data acquisition at mid-diastole. We implemented an MPI pulse sequence that acquires 3D perfusion data set at both end-systole and mid-diastole and performed a comparison of perfusion images and region-based time-intensity curves (TICs) from the two cardiac phases. In order to achieve complete LV coverage, we used a relatively low spatial resolution, which is more likely to suffer from dark rim artifacts (14) and may be incapable of identifying small perfusion defects. In this pilot study, we studied only healthy subjects with no known perfusion defect. We hypothesize that systolic 3D MPI and diastolic 3D MPI will provide comparable myocardial resolution and semiquantitative perfusion

[1]Ming Hsieh Department of Electrical Engineering, University of Southern California, Los Angeles, California, USA.

[2]Keck School of Medicine, University of Southern California, Los Angeles, California, USA.

Grant sponsor: Department of Energy; Grant number: DE-FG02-05ER64128.

*Correspondence to: Taehoon Shin, Ph.D., 3740 McClintock Ave, EEB 408, University of Southern California, Los Angeles, CA 90089-2564. E-mail: shinage@gmail.com

Received 2 May 2009; revised 2 November 2009; accepted 6 November 2009.

DOI 10.1002/mrm.22315
Published online in Wiley InterScience (www.interscience.wiley.com).

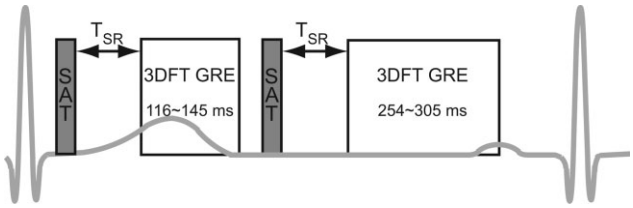

FIG. 1. Schematic of pulse sequence for systolic and diastolic 3D MPI. The pulse sequence consists of two sets of saturation RF pulse followed by a delay (T_{SR}) and 3DFT Gradient echo (GRE) readout. The centers of two data acquisitions were located at end-systole and mid-diastole. The largest possible T_{SR} was used with a maximum threshold of 120 ms, depending on a given heart rate.

indices, and thus systolic imaging may be favorable in subjects with severe R-R variability.

MATERIALS AND METHODS

Pulse Sequence

The pulse sequence consisted of two saturation recovery 3DFT acquisition modules, one at end-systole and the other at mid-diastole (Fig. 1). This enabled systolic and diastolic perfusion data to be acquired during the same R-R interval from a single injection of contrast agent, avoiding potential issues related to residual contrast and physiologic changes that could occur between two separate scans. For the preparatory saturation, we used a tailored hard-pulse train that is robust in the presence of amplitude of static and radiofrequency (RF) fields and inhomogeneities and involves relatively low RF power (15). A sinc-shaped RF pulse with a time-bandwidth product of 4 was used for slab selective excitation. A cine balanced SSFP scan was used to identify the centers of the stable end-systolic and mid-diastolic phases. These centers were recorded as a fraction relative to the total R-R interval duration (e.g., if the R-R interval was 1000 ms, and the centers of the stable phases were 300 ms and 700 ms after the trigger, then 30% and 70% were recorded). During the perfusion scan, the trigger delays were prospectively updated every cardiac cycle, based on the recorded percentages and the duration of the immediately previous R-R interval. In this way, the acquisitions will occur during stable phases unless there is a sudden and large change in heart rate.

3D *k*-space for given field of view and spatial resolution was undersampled by factor of 3 and 2 along k_y and k_z directions, e.g., by a net factor of 6, in both systolic and diastolic imaging. The position of sampled *k*-space encoding lines was shifted in a cyclic pattern such that the data acquired from six neighboring cardiac cycles can be combined to generate a coil sensitivity map for sensitivity encoding reconstruction (16,17).

Imaging Protocols

The imaging parameters are summarized in Table 1. We used a shorter data acquisition window for systolic imaging due to its shorter quiescent period. We used a lower in-plane resolution and a smaller number of partition slices. This choice was motivated by the fact that, in general, systolic myocardium is transmurally thicker and is shorter along the long axis. The number of partition slices also depended on the subject's heart rate, with a threshold of 85–90 beats/min. Saturation recovery time T_{SR}, defined as the time interval between the end of saturation RF pulse and the start of data acquisition, was limited by the R-R interval. The pulse sequence used the longest possible T_{SR} within a maximum value of 120 ms. The acquisition of systolic and diastolic data in the same R-R limits the saturation recovery time for diastolic imaging, resulting in slightly reduced Contrast-to-noise ratio (CNR). Based on Bloch simulation, the CNR reduction is less than 20% for heart rates between 50 and 120 beats/min. The systolic scan volume is shifted toward the apex by 8–10 mm relative to the diastolic scan volume.

3D MPI experiments were performed in five healthy subjects (sex: three female/two male; age: 21–55 years), using Generic Electric 3 Tesla scanner and an eight-channel cardiac coil. Prior to perfusion scans, SSFP cine images were obtained for the determination of the centers of the two acquisition windows. Contrast agent (0.05 mmol/kg Gd-DTPA; Magnevist) was injected at a rate of 4 mL/sec 0–5 sec before the start of scan. Subjects were instructed to hold their breath as long as possible.

Image Reconstruction and Analysis

All image reconstruction and subsequent analysis were implemented offline in MATLAB (Mathworks, Natick, MA). Two-dimensional TSENSE was used for image reconstruction from undersampled 3DFT perfusion data from the two cardiac phases (16,17). The data from six

Table 1
Imaging Parameters for Systolic and Diastolic 3D MPI Data Acquisition

	Systolic imaging		Diastolic imaging	
	Low HR	High HR	Low HR	High HR
Matrix size[a]	62 × 42 × 8	62 × 42 × 6	100 × 66 × 10	100 × 66 × 8
Field of view (cm^3)	28 × 28 × 8	28 × 28 × 6	28 × 28 × 10	28 × 28 × 8
Acquisition time (ms)	144.8	115.8	304.7	253.9
Pulse repetition time/echo time (ms)	2.1/0.9		2.3/1.0	
Flip angle (degree)	12		12	

[a]The third dimension represents the number of partition slices after discarding one slice from each edge. In other words, the number of k_z phase encodes that were acquired is this number plus 2.

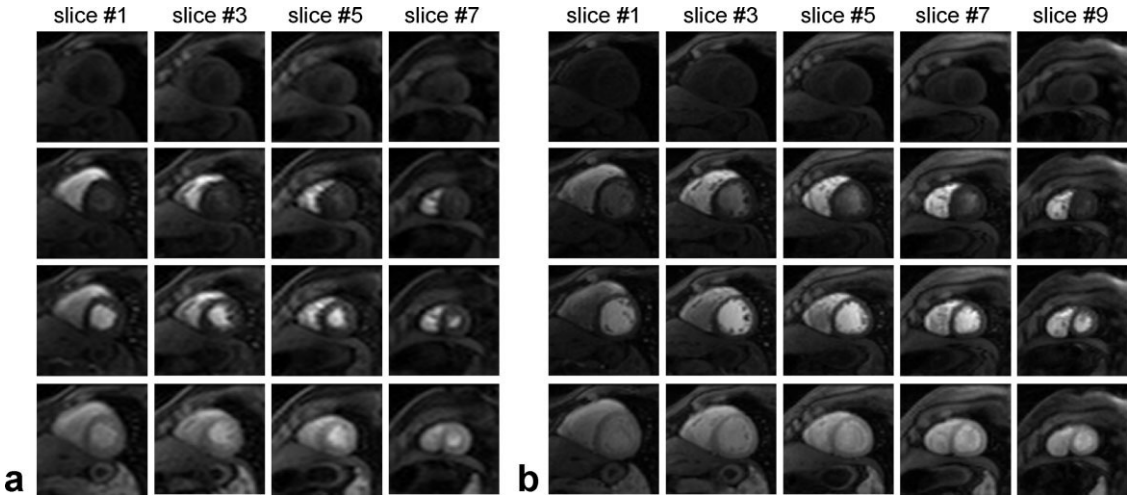

FIG. 2. Representative **(a)** systolic and **(b)** diastolic 3D perfusion images from a healthy subject at precontrast, right ventricle enhancement, LV enhancement, and myocardial enhancement. The passage of contrast agent is captured with complete myocardial coverage and high image quality. Despite the difference in spatial resolution, systolic and diastolic images provide comparable transmural resolution (in pixel units).

neighboring heartbeats were combined to form coil sensitivity maps.

All perfusion images were normalized by precontrast images obtained by combining data from the first six cardiac cycles to correct for the effects of different T_{SR} and receiver coil sensitivities. From the normalized images, endocardial and epicardial contours were manually segmented. Myocardium was then automatically subdivided into endocardial and epicardial layers and six azimuthal sectors to generate time TICs from a total of 12 segments per slice. Upslope and peak enhancement values were calculated for each myocardial segment and were normalized by an upslope from the LV to compensate for intersubject variation.

Systolic and diastolic data sets were manually registered, and the four partition slices closest to the mid-short axis level were used for TIC similarity analyses on a segment-by-segment basis. First, correlation coefficient between systolic and diastolic TICs was calculated to measure the similarity of overall dynamics in TICs. Second, TIC upslope and peak enhancement were compared to measure the similarity between semiquantitative perfusion indices. A total of 240 segments were analyzed in five subjects (48 segments per subject).

RESULTS

Example systolic and diastolic 3D perfusion images from one subject are shown in Fig. 2. Images from both cardiac phases show complete myocardial coverage and diagnostic image quality with high SNR. Both image sets suffer from slight dark rim artifacts during LV enhancement. The dark rim is slightly thicker in the systolic images, presumably due to their lower in-plane resolution (14). The myocardial wall thickness in "pixel units" was similar for systolic and diastolic cardiac phases (Table 2). The wall thickness was measured as 3.35 ± 0.52 (systole) versus 3.30 ± 0.49 (diastole) in anterior and inferior walls and 2.27 ± 0.45 versus 2.29 ± 0.48 in septal and lateral walls. The transmural resolution is higher in the anterior and inferior walls compared to the septal and lateral walls because the acquisition has asymmetric spatial resolution, and the anterior-inferior direction is more closely aligned with the (higher resolution) frequency-encoding direction.

Figure 3 shows representative systolic and diastolic TICs from the four partition slices closest to the mid-short axis level. All myocardial segments exhibit homogeneous signal enhancement, indicating normal perfusion.

Table 2
Systolic and Diastolic Myocardial Thicknesses, Measured in Pixel Units

	Systolic myocardium		Diastolic myocardium	
	Anterior/inferior	Septal/lateral	Anterior/inferior	Septal/lateral
Subject 1	3.10/3.41	1.89/2.10	3.00/4.00	1.65/2.31
Subject 2	3.72/4.34	2.94/2.52	3.50/3.50	1.98/2.64
Subject 3	3.72/3.41	2.94/2.31	2.50/4.00	2.97/2.97
Subject 4	3.41/3.10	1.89/2.52	3.00/3.50	1.98/2.64
Subject 5	2.64/2.64	1.89/1.68	2.75/3.25	1.82/1.98
All	3.35 ± 0.52	2.27 ± 0.45	3.30 ± 0.49	2.29 ± 0.48

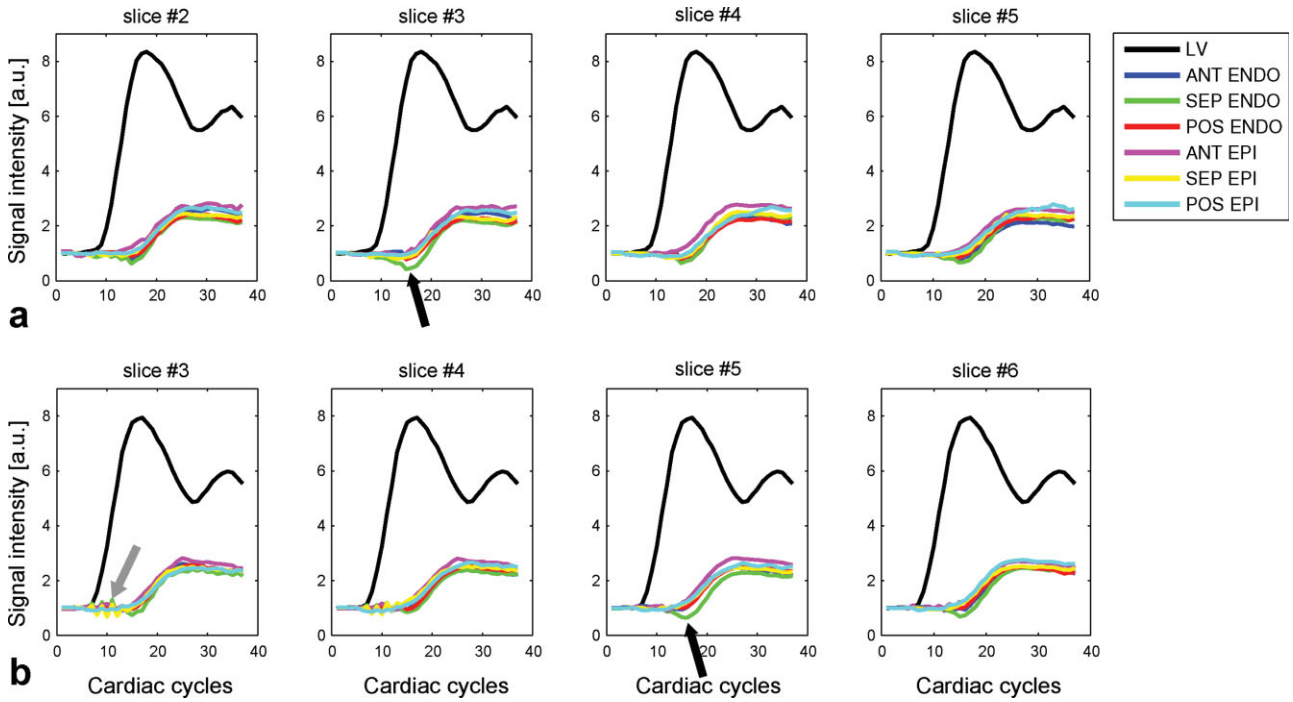

FIG. 3. Representative TICs based on **(a)** systolic and **(b)** diastolic perfusion images from a healthy subject. Homogeneous signal enhancement is observed in nearly all myocardial segments. Diastolic slice #3 suffered from flickering artifacts caused by errors in coil sensitivity map estimation (see gray arrow). Some endocardial TICs exhibit a signal dip (see black arrows) that is temporally aligned with peak LV enhancement and is likely to be related to dark rim artifact.

Some endocardial TICs show a signal dip (indicated by the black arrows) that is temporally aligned with peak LV enhancement and is likely to be related to dark rim artifact. TICs in one diastolic basal slice suffer from fluctuation (indicated by the gray arrow) that temporally corresponds to rapid signal elevation in LV and is related to aliasing artifacts in the TSENSE coil sensitivity maps estimated by sliding window reconstruction.

Figures 4 and 5 contain the results of a similarity analysis between systolic and diastolic TICs. The average and standard deviation of the correlation coefficients between the two sets of TICs were 0.9841 and 0.0166 across all 240 segments (Fig. 4). The mean values were larger than 0.97 in all five subjects, indicating excellent correlation between temporal dynamics of the two sets of TICs. Figure 5 contains scatter plots of the TIC upslope and peak enhancement values of the systolic and diastolic data and results of linear fitting. The linear correlations between the two sets of upslope and peak enhancement values were significant ($P < 0.001$ in both).

Figure 6 compares endocardial and epicardial layers in terms of TIC upslope and peak enhancement. There was no significant difference in either upslope or peak enhancement between the endocardial and epicardial layers. This was true for both systolic and diastolic data across all subjects (at $P = 0.05$). The average upslope was slightly larger in the endocardial layer, likely due to dark rim artifact that is reduced as LV signal decreases (see Fig. 3). The ratio of average endocardial to epicardial upslopes was 1.0539 and 1.0741 in the systolic and diastolic TICs, respectively. The average peak enhancement was slightly smaller in the endocardial layer, likely due to the residual effects of elevated LV blood pool signal. The ratio of average endocardial to epicardial peak enhancement values was 0.9557 and 0.9580 in the systolic and diastolic TICs, respectively.

DISCUSSION

We have demonstrated the feasibility of systolic 3D MPI, and the equivalence of TICs derived from systolic versus

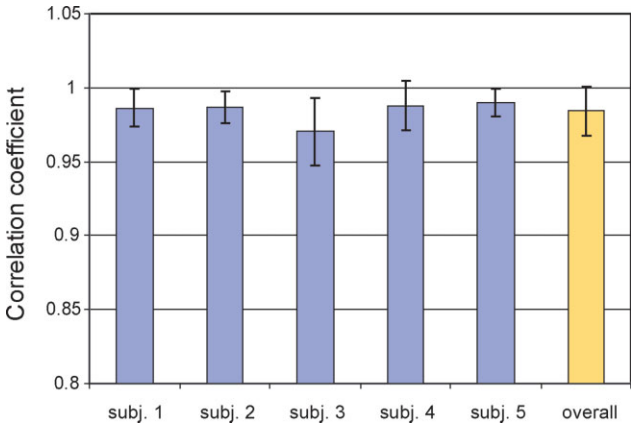

FIG. 4. Correlation coefficients between systolic and diastolic TICs. Mean and standard deviation of the coefficient were 0.9841 and 0.0166 across a total of 240 segments in five subjects (48 segments per subject), and mean coefficient was larger than 0.97 in all five subjects, which validates strong similarity between overall dynamics in the two sets of TICs. [Color figure can be viewed in the online issue, which is available at www.interscience.wiley.com.]

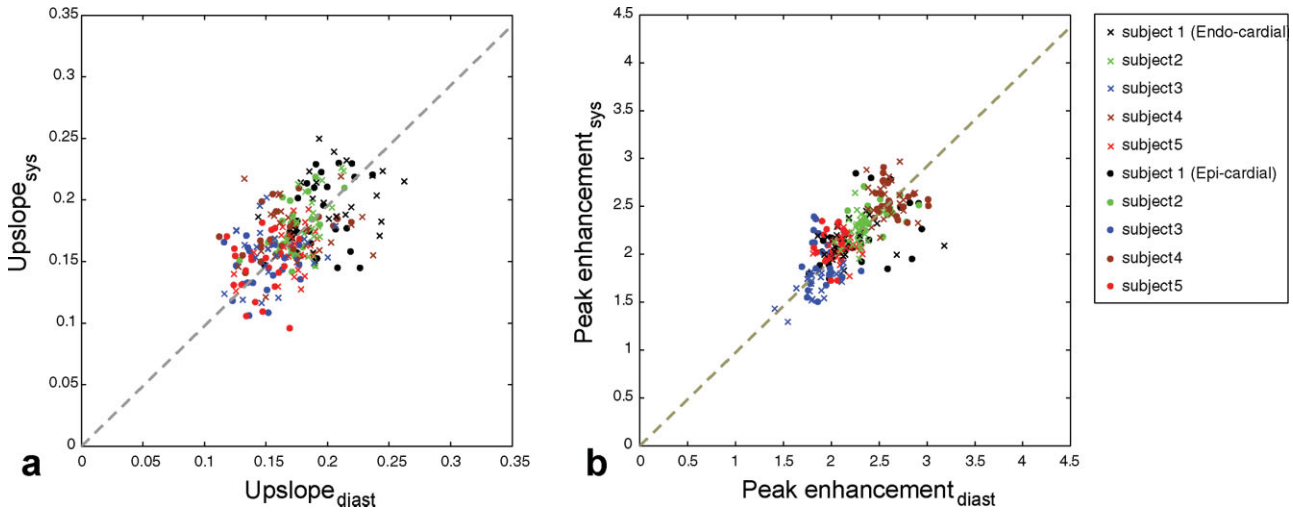

FIG. 5. Scatter plot of TIC **(a)** upslope and **(b)** peak enhancement for diastolic and systolic acquisitions. Linear fitting across all myocardial segments results in y = 0.9768x ($P < 0.001$) and y = 0.9728x ($P < 0.001$) for upslope and peak enhancement, respectively. [Color figure can be viewed in the online issue, which is available at www.interscience.wiley.com.]

diastolic acquisitions, in healthy subjects. Region-based TICs from systolic images were shown to be highly correlated with those from diastolic images in terms of overall temporal dynamics, upslope, and peak enhancement. We found no statistically significant difference between the upslope and peak enhancement values obtained from endocardial and epicardial segments. On average, upslope was slightly larger and peak enhancement was slightly lower in the endocardial layer than in the epicardial layer, likely due to dark rim artifact. This interlayer

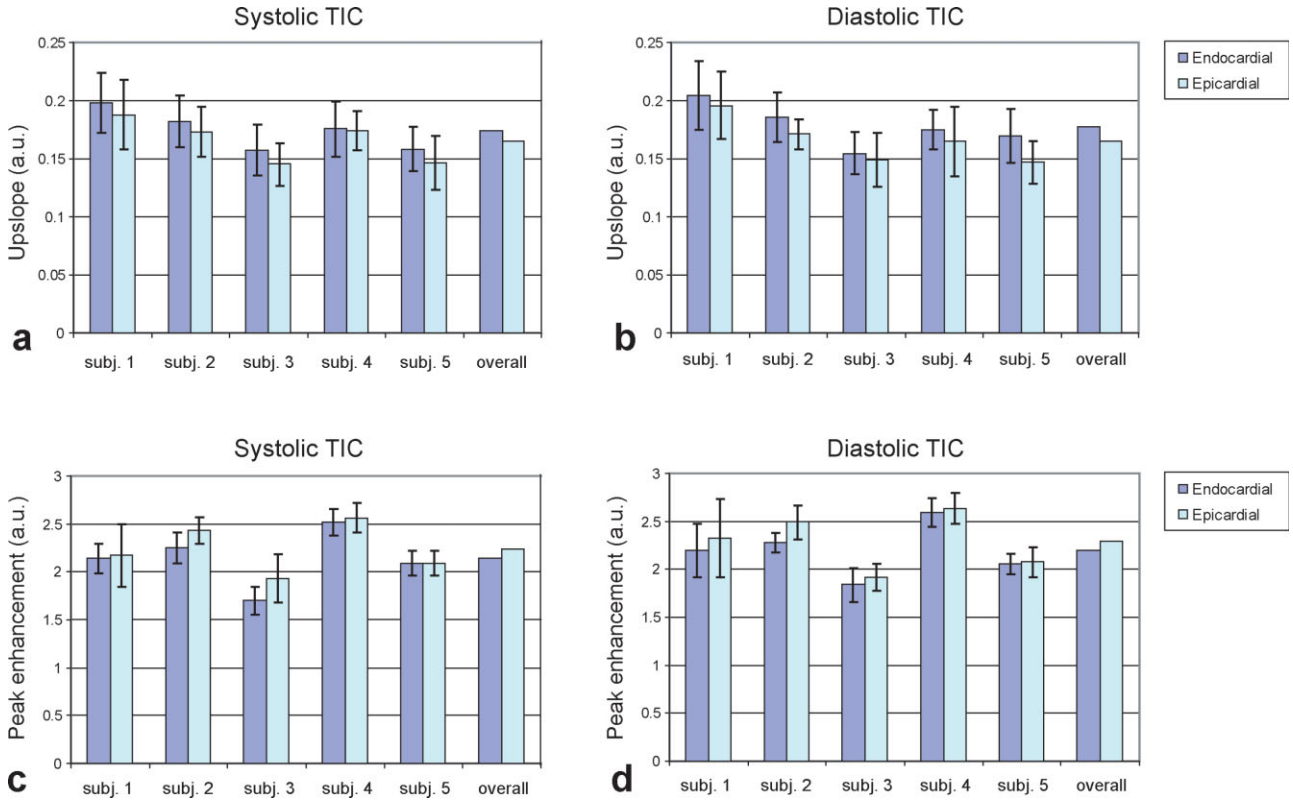

FIG. 6. Comparison of time curve upslope and peak enhancement between endocardial and epicardial layers: **(a)** systolic upslope, **(b)** diastolic upslope, **(c)** systolic peak enhancement, and **(d)** diastolic peak enhancement. The difference of upslope and peak enhancement between two layers was statistically insignificant in both systolic and diastolic data (at $P = 0.05$). The ratio of average endocardial to epicardial upslopes was 1.0539 and 1.0741 in the systolic and diastolic TICs, respectively. The ratio of average endocardial to epicardial peak enhancement values was 0.9557 and 0.9580 in the systolic and diastolic TICs, respectively. [Color figure can be viewed in the online issue, which is available at www.interscience.wiley.com.]

difference was similar for both cardiac phases, presumably due to similar myocardial thickness in pixel units.

A shorter data acquisition was used for the systolic phase due to its shorter quiescent period. We chose to accomplish this by reducing spatial resolution, based on the notion that myocardium is transmurally thicker in systole than in diastole. Across the five healthy subjects, the average systolic and diastolic wall thicknesses were 15.1 mm and 9.5 mm, respectively. With the proposed approach, both cardiac phases achieved similar transmural resolution in "pixel units" (Table 2), which suggests that both phases may have similar ability to detect nontransmural perfusion defects. Patients with severe irreversible defects may suffer from reduced systolic wall thickening (18), which will decrease transmural spatial resolution in affected segments. The incidence and degree of wall-thickening impairment should be investigated in patients with ischemic heart disease. Despite the use of the two most stable cardiac phases, these acquisitions are longer than individual image acquisition times used with the traditional 2D multislice approach and may experience more significant motion artifacts. Further investigation is needed to characterize and minimize motion artifacts in 3D MPI.

One limitation of this study is the use of relatively low spatial resolution, which is more likely to suffer from dark rim artifacts and may be incapable of identifying small perfusion defects. This is an important consideration and needs to be investigated in patients with known perfusion defects. At this time, dark rim artifacts are the most significant limitation to the clinical acceptance of MR MPI, which underscores the need to achieve higher spatial resolution. This may be achieved through the use of higher acceleration, including use of high-density coil arrays and high-rate parallel imaging, and/or regularized reconstruction (19,20).

Flickering artifacts were seen in both systolic and diastolic perfusion images, especially when viewed in video format. This artifact is caused by errors in coil sensitivity maps that are derived from six neighboring cardiac cycles and thus suffers from aliasing during rapid signal change. Across temporal frames, the flickering is the most severe during the arrival of contrast agent into the right ventricle and LV, appearing as fluctuation in time curves (Fig. 3). This had a negligible effect on the overall myocardial TIC upslopes since the signal enhancement in blood pool precedes myocardial enhancement. Variable-density *k*-space trajectories and keyhole reconstruction for coil map generation may reduce and diffuse the artifacts over the field of view (21,22).

The TIC upslope has shown variation across myocardial segments and subjects in both systolic (0.1699 ± 0.0223) and diastolic data (0.1717 ± 0.0212). The corresponding percentage standard deviation (13.1% and 12.3% for systolic and diastolic upslope, respectively) was lower than standard deviation reported in previous studies (18.1%-25.8%; (23,24)). Potential reasons for this variation include spatial variation in image intensity due to receiver coil sensitivity, transmit RF inhomogeneity, and the slab excitation profile. Normalization by precontrast images should have corrected for most of the variation yet were not perfect. The diagnostic value of the TIC upslope as a semiquantitative perfusion index will be valid only if the upslope distribution of normal and defected myocardium is well separated. This separability should be further confirmed in patients with perfusion defects.

CONCLUSIONS

The feasibility of systolic 3D MPI has been demonstrated in healthy subjects. Myocardial signal enhancement captured by systolic 3D imaging has been shown to be comparable to diastolic 3D imaging by region-based TIC analysis. The mean and standard deviation of the correlation coefficients between systolic and diastolic TICs were 0.9841 and 0.0166, and the linear correlation between the two sets of TIC upslope and peak enhancement values was statistically significant ($P < 0.001$). Systolic 3D MPI may be advantageous in subjects with severe R-R variability.

ACKNOWLEDGMENTS

The authors thank Dr. Padmini Varadarajan and Dr. Ramdas G. Pai for useful discussions and collaboration.

REFERENCES

1. Wolff SD, Schwitter J, Coulden R, Friedrich MG, Bluemke DA, Biederman RW, Martin ET, Lansky AJ, Kashanian F, Foo TK, Licato PE, Comeau CR. Myocardial first-pass perfusion magnetic resonance imaging: a multicenter dose-ranging study. Circulation 2004;110: 732–737.
2. Plein S, Radjenovic A, Ridgway JP, Barmby D, Greenwood JP, Ball SG, Sivananthan MU. Coronary artery disease: myocardial perfusion MR imaging with sensitivity encoding versus conventional angiography. Radiology 2005;235:423–430.
3. Shin T, Hu HH, Pohost GM, Nayak KS. Three-dimensional first-pass myocardial perfusion imaging at 3T: feasibility study. J Cardiovasc Magn Reson 2008;10:57.
4. Yokota H, Heidary S, Katikireddy CK, Nguyen P, Pauly JM, McConnell MV, Yang PC. Quantitative characterization of myocardial infarction by cardiovascular magnetic resonance predicts future cardiovascular events in patients with ischemic cardiomyopathy. J Cardiovasc Magn Reson 2008;10:17.
5. Brown KA, Boucher CA, Okada RD, Guiney TE, Newell JB, Strauss HW, Pohost GM. Prognostic value of exercise thallium-201 imaging in patients presenting for evaluation of chest pain. J Am Coll Cardiol 1983;1:994–1001.
6. Hachamovitch R, Berman DS, Shaw LJ, Kiat H, Cohen I, Cabico JA, Friedman J, Diamond GA. Incremental prognostic value of myocardial perfusion single photon emission computed tomography for the prediction of cardiac death. Circulation 1998;97:535–543.
7. Marwick TH, Case C, Sawada S, Rimmerman C, Brenneman P, Kovacs R, Short L, Lauer M. Prediction of mortality using dobutamine echocardiography. J Am Coll Cardiol 2001;37:754–760.
8. Kellman P, Zhang Q, Larson AC, Simonetti OP, McVeigh ER, Arai AE. Cardiac first-pass perfusion MRI using 3D true FISP parallel imaging using TSENSE. In: Proceeding of ISMRM 12th Annual Meeting, Kyoto, 2004. p 310.
9. Johnson KR, Patel SJ, Whigham A, Hakim A, Pettigrew RI, Oshinski JN. Three-dimensional, time-resolved motion of the coronary arteries. J Cardiovasc Magn Reson 2004;6:663–673.
10. Gharib AM, Herzka DA, Ustun AO, Desai MY, Locklin J, Pettigrew RI, Stuber M. Coronary MR angiography at 3T during diastole and systole. J Magn Reson Imaging 2007;26:921–926.
11. Weissler AM, Harris WS, Schoenfeld CD. Systolic time intervals in heart failure in man. Circulation 1968;37:149–159.
12. Furberg CD, Psaty BM, Manolio TA, Gardin JM, Smith VE, Rautaharju PM. Prevalence of atrial fibrillation in elderly subjects (the Cardiovascular Health Study). Am J Cardiol 1994;74:236–241.

13. Benjelloun H, Itti R, Philippe L, Lorgeron JM, Brochier M. Beat-to-beat assessment of left ventricular ejection in atrial fibrillation. Eur J Nucl Med 1983;8:206–210.
14. Di Bella EVR, Parker DL, Sinusas AJ. On the dark rim artifact in dynamic contrast-enhanced MRI myocardial perfusion studies. Magn Reson Med 2005;54:1295–1299.
15. Sung K, Nayak KS. The design and use of tailored hard-pulse trains for uniform saturation of myocardium at 3 tesla. Magn Reson Med 2008;60:997–1002.
16. Weiger M, Pruessmann KP, Boesiger P. 2D SENSE for faster 3D MRI. MAGMA 2002;14:10–19.
17. Kellman P, Epstein FH, McVeigh ER. Adaptive sensitivity encoding incorporating temporal filtering (TSENSE). Magn Reson Med 2001;45:846–852.
18. Perrone-Filardi P, Bacharach L, Dilsizian V, Maurea S, Frank JA, Bonow RO. Regional left ventricular wall thickening: relation to regional uptake of ^{18}fluorodeoxyglucose and 201Tl in patients with chronic coronary artery disease and left ventricular dysfunction. Circulation 1992;86:1125–1137.
19. Liu B, King K, Steckner M, Xie J, Sheng J, Ying L. Regularized sensitivity encoding (SENSE) reconstruction using Bregman iterations. Magn Reson Med 2009;61:145–152.
20. Block KT, Uecker M, Frahm J. Undersampled radial MRI with multiple coils: iterative image reconstruction using a total variation constraint. Magn Reson Med 2007;57:1086–1098.
21. van Vaals JJ, Brummer ME, Dixon WT, Tuithof HH, Engels H, Nelson RC, Gerety BM, Chezmar JL, den Boer JA. Keyhole method for accelerating imaging of contrast agent uptake. J Magn Reson Imaging 1993;3:671–675.
22. Jones RA, Haraldseth O, Muller TB, Rinck PA, Oksendal AN. k-Space substitution: a novel dynamic imaging technique. Magn Reson Med 1993;29:830–834.
23. Sipola P, Lauerma K, Husso-Saastamoinen M, Kuikka J, Vanninen E, Laitinen T, Manninen H, Niemi P, Peuhkurinen K, Jääskeläinen P, Laakso M, Kuusisto J, Aronen H. First-pass MR imaging in the assessment of perfusion impairment in patients with hypertrophic cardiomyopathy and the Asp175Asn mutation of the alpha-tropomyosin gene. Radiology 2003;226:129–137.
24. Panting JR, Gatehouse PD, Yang G-Z, Grothues F, Firmin DN, Collins P, Pennell DJ. Abnormal subendocardial perfusion in cardiac syndrome X detected by cardiovascular magnetic resonance imaging. N Engl J Med 2002;346:1948–1953.